analytical chemistry

Article

pubs.acs.org/ac

Tiny Peaks vs Mega Backgrounds: A General Spectroscopic Method with Applications in Resonant Raman Scattering and Atmospheric Absorptions

Baptiste Auguié,[†] Antoine Reigue,[†,‡] Eric C. Le Ru,*[,†] and Pablo G. Etchegoin*[,†]

[†]The MacDiarmid Institute for Advanced Materials and Nanotechnology, School of Chemical and Physical Sciences, Victoria University of Wellington, PO Box 600, Wellington, 6140, New Zealand

[‡]ICFP, Département de Physique de l'ENS, 24 rue Lhomond, 75005 Paris, France

Supporting Information

ABSTRACT: A simple method using standard spectrometers with charge-coupled device (CCD) detectors is described to routinely measure background-corrected spectra in situations where the signal is composed of weak spectral features (such as Raman peaks or absorption lines) engulfed in a much stronger (by as much as ~10^5) broad background. The principle of the method is to subtract the dominant fixed-structure noise and obtain a shot-noise limited spectrum. The final noise level can therefore be reduced as desired by sufficient integration time. The method requires multiple shifts of the diffraction gratings to extract the pixel-dependent noise structure, which is then used as a flat-field correction. An original peak-retrieval procedure is proposed, demonstrating accurate determination of peak lineshapes and linewidths and robustness on practical examples where conventional methods would not be applicable. Examples are discussed to illustrate the potential of the technique to perform routine resonant Raman measurements of fluorescent dyes with high quantum yield, using conventional Raman systems. The method can equally be applied to other situations where small features are masked by a broad overwhelming background. An explicit example is given with the measurement of weak absorption lines in atmospheric gases.

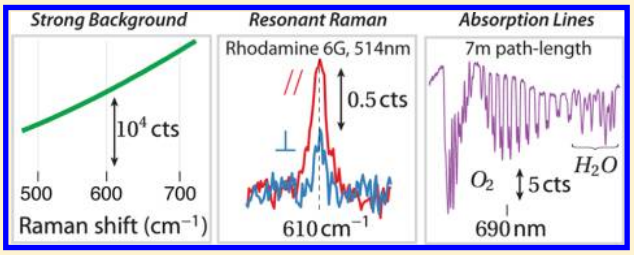

Detecting very small signals on top of large underlying backgrounds has always been a holy grail in optical spectroscopy, and over the years, several methods have been developed for that purpose.[1−24] The different methods use a combination of hardware and data analysis tricks to achieve the stated goal, and they differ in the ultimate level of background rejection that can be achieved. The particular spectroscopic problems that these methods can potentially address are multiple, but a longstanding and canonical example is fluorescence rejection in resonant Raman (RR) spectroscopy.[25,26]

In fact, the challenge of fluorescence rejection in Raman spectroscopy has a long history that goes back to the '70s and '80s with scanning instruments and polarization modulation with lock-in amplifiers.[27,28] Modest rejection of extrinsic fluorescence backgrounds of the order of ~10^{-1}−10^{-2} (signal with respect to background) were reported at the time. A game-changer in Raman spectroscopy occurred with the advent of charge-coupled device (CCD) detectors in the mid-to-late '80s,[29] and background rejection methods adapted to the new capabilities of the detector. Broadly speaking, three classes of strategies have been developed for that purpose. The first type of methods focus on data postprocessing to fit and subtract the unwanted backgrounds.[10,11] The main limitation of this approach is that it does not address the crucial problem of removing the noise associated with the large background signal (this noise is typically much larger than the signal we wish to retrieve). The second approach attempts to solve this issue by reducing the intensity of the background (and therefore the associated noise), for example using lock-in methods. Time-resolved techniques,[24,30−34] which exploit the fact that Raman scattering is instantaneous while fluorescence is slightly delayed, have undoubtedly been the most successful in this category, but they come at the expense of increased complexity. The third category consists of spectrum subtraction methods, designed to remove any fixed noise associated with the background and therefore obtain shot-noise (photon-noise) limited spectra. With sufficient integration time, the shot-noise level can be reduced to the point where the Raman peaks can be revealed with standard background-subtraction postprocessing. The two main techniques in this category are (i) shifted excitation Raman difference spectroscopy (SERDS),[17−19,35] which consists of the use of two (closely spaced) laser excitation wavelengths and taking difference spectra, and (ii) subtracted-shifted Raman spectroscopy (SSRS),[2−6] which instead takes the difference between two spectra obtained at two (closely spaced) spectrometer shifts. These two methods have been

Received: June 20, 2012
Accepted: August 15, 2012
Published: August 15, 2012

   dx.doi.org/10.1021/ac301696p | Anal. Chem. 2012, 84, 7938−7945

used in a variety of applications, yet no demonstration has been proposed at the levels of sensitivity required for resonant Raman measurements with medium-to-high quantum yield fluorophores (over ∼1%). Additionally, the general applicability of SERDS and SSRS suffers from the inconvenience that they both retrieve a difference-spectrum (akin to the derivative spectrum); recovering the original Raman spectrum typically requires assumptions on the lineshapes of the Raman peaks.

Our group recently introduced a new method, polarization difference resonant Raman spectroscopy (PD-RRS),[36] based on the subtraction of two spectra obtained with different polarization configurations. This method does not require any assumption on the peak lineshapes and, crucially, was shown to be sensitive enough to measure RR spectra in some of the most challenging situations, such as the dye Rhodamine 6G (RH6G) excited at 514 nm. However, PD-RRS suffers an intrinsic limitation in that it requires the Raman signal to be polarization dependent (at least to a greater extent than fluorescence). This is not an issue in the majority of cases but precludes the general use of the method in other polarization-independent applications. It also means that PD-RRS cannot be used to study the polarization properties of the Raman signal, in particular to measure depolarization ratios at resonance.

Overall, despite the relative success of these techniques, no attempts have been made, with the recent exception of our work on PD-RRS,[36] to tackle the most challenging high-quantum yield fluorescent dyes in full resonance, with conventional Raman systems. Most attempts to remove fluorescent backgrounds in the past have only considered controlled extrinsic fluorescence, and in most cases, the Raman peaks could still be distinguished above the background as faint but nevertheless discernible features. The case of high-quantum yield fluorescent dyes is conventionally considered to be out of reach of standard Raman spectroscopy[14] and has only been addressed recently using much more sophisticated time-resolved[24] or nonlinear (stimulated) spectroscopies.[30−34] Even with these advanced methods, RR measurements remain very challenging. In fact, the first results for the Raman cross-section of RH6G were published in 2008,[30] using an experimental setup that is not commonly available.

This is the situation we set out to challenge in this work with a novel general method based on a refined implementation of SSRS, or shifted-grating spectroscopy, demonstrating record levels of sensitivity that allow us to extract Raman cross sections and even depolarization ratios in full resonance conditions with a conventional Raman spectrometer. Our results here are to some extent a generalization of our work presented in ref 36, which works for polarized signals only (of which resonant Raman scattering is an example). The method presented here, in contrast, allows us to measure depolarization ratios even for dyes with ∼100% quantum yield in full resonance and is also better suited to measurements of complete RR spectra. Furthermore, the method can be applied to other situations where small signals are to be resolved in a large background, irrespective of whether the depolarization ratios differ. We show an example with the measurement of weak absorption lines of atmospheric gases, finely resolving the structure of the (Fraunhofer) B-band of oxygen[37] with a conventional spectrometer and a very short optical path length (∼ meters) compared to the ones commonly considered for such measurements in atmospheric physics (∼ kilometers).

PRINCIPLE OF THE METHOD

The signal-to-noise ratio, which limits the detection level of Raman peaks in the fluorescence background, can be improved by averaging over many spectra for as long as it is dominated by shot (photon) noise. However, as explained in detail in ref 36, this procedure rapidly reveals a major obstacle: the presence of a fixed-structure, or fixed-pattern noise,[29] which is proportional to the signal intensity (fluorescence), and therefore is independent (in relative terms) of the photon counts. This limits the detectable signals to Raman-to-background ratios above typically $\sim 10^{-2}-10^{-3}$.

The relative rms noise, ε, has two contributions relevant to our experiment: a constant fixed structure characterizing the nonuniform response of CCD columns of pixels (this contribution is independent of the number of acquired photons) and the photon-limited shot noise, scaling as the inverse square root of the number of acquired spectra[36] (this is illustrated in Figure SI1 of the Supporting Information). The photon-limited noise is an intrinsic physical hurdle for any optical scattering process such as Raman and can be overcome by increasing the number of acquired photons (with a detrimental effect on the time-scale of the acquisition). In order to reach a level of relative rms below $\varepsilon \approx 10^{-3}$ required in challenging resonant Raman experiments, the fixed structure noise has to be eliminated by other means, as it is independent of the number of collected photons. One way to remove this fixed-structure noise is to measure it for a well-defined flat-field intensity (we note here that what we call flat-field here is not necessarily exactly spectrally flat but may have any broad smooth spectral shape, affected by the fixed-structure noise). If such a flat-field correction scheme can be devised to eliminate the fixed-structure contribution from the CCD counts, the acquisition of multiple spectra will regain photon-limited statistics, whereby the relative rms noise and therefore the detectable Raman-to-fluorescence ratio can be improved by 2 orders of magnitude to at least $\sim 10^{-5}$, as we shall demonstrate in this Article.

Both SERDS and SSRS methods implement a basic version of such a flat-field correction, simply using a shifted Raman spectrum as reference for the flat-field, as illustrated in Figure 1a. However, because Raman peaks are present in this flat-field spectrum, they produce negative peaks in the corrected spectrum, which therefore appears as a derivative-like or difference Raman spectrum. The new method we propose here aims at removing or strongly reducing this Raman peak contribution in the flat-field spectrum. This can be achieved by averaging (along each CCD bin) the spectra obtained for many small shifts of the gratings (typically about 50 shifts of 2 cm^{-1}, rather than a single shift of ∼20 cm^{-1} in SSRS). Such averaging flattens out the Raman peak contribution to the flat-field spectrum, as illustrated in Figure 1c (bottom left). The subsequent data analysis differs substantially from SSRS, in order to exploit the multiple spectra obtained for individual grating shifts. The flat-field spectrum is first used to remove the fixed-structure noise from each of these individual spectra as shown in Figure 1c (bottom right). The resulting flat-field corrected spectra contain the Raman peaks, but no fixed-structure noise, and can therefore be averaged (this time along each Raman shift) to obtain the average flat-field corrected Raman spectrum. This method will be referred to with the acronym ffc-CSRS, for flat-field corrected continuously shifted Raman spectroscopy. The detailed technical implementation

dx.doi.org/10.1021/ac301696p | Anal. Chem. 2012, 84, 7938−7945

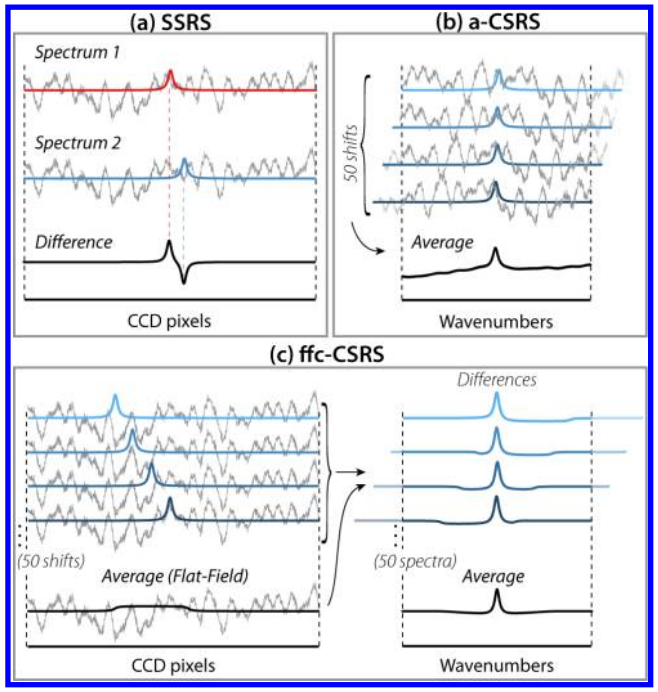

Figure 1. Principle of the SSRS, ffc-CSRS, and a-CSRS methods. Simulated spectra are decomposed into fluorescence background (not shown), fixed-structure noise (gray lines), and Raman signals (color lines). (a) In the shifted-subtracted Raman spectroscopy (SSRS) method, the difference is taken between two spectra recorded with a shift of ~20 cm^{-1}. (b) With the averaged-continuously shifted Raman spectroscopy (a-CSRS) method, a number of spectra are recorded with small shifts (typically ~50 shifts of 2 cm^{-1}). The average spectrum, in the region of overlapping wavenumbers, decreases the fixed structure noise due to the inhomogeneous response of the CCD array. (c) In the flat-field corrected version (ffc-CSRS), multiple spectra are first averaged along the corresponding pixel column, resulting in a flat-field spectrum that contains the fixed-structure noise of the CCD plus a minute distortion from the multiply shifted repetitions of the Raman spectrum. In the following step, the flat-field correction is subtracted from each spectrum, thus removing the fixed structure, and the resulting differences are averaged in the overlapping region of wavenumbers.

and data processing of ffc-CSRS are further described in the Supporting Information.

It is interesting to note that the method bears some resemblance with the so-called Kiefer scanning,[38] which was developed to improve the resolution of Raman spectra.[29] This method also consists in measuring Raman spectra for many small shifts of the grating and carrying out a simple averaging (at given Raman shifts) of the observed spectra. This results in a smoothing of the fixed-structure noise, as shown in Figure 1b, and therefore allows one to reduce to some extent (but not entirely) this noise contribution. The reason for this reduction of the fixed structure is that in the shifted spectra each Raman shift appears at a different pixel. Hence, by averaging the realigned spectra, we are effectively averaging (at least partially) the fixed-structure noise of different pixels. In fact, if each wavelength goes through the 1024 pixels of the CCD by shifting the grating 1024 times, each sampled wavelength would accumulate the same average fixed-structure noise, thus removing it entirely. In practice, however, small variations of the fixed-structure noise for large grating shifts are likely to result in additional imperfections. We will therefore restrict our studies to small total shifts of typically 50−100 cm^{-1}. This approach based on Kiefer scanning can also be used for resonant Raman spectroscopy, even if it was not its intended primary use. It differs from ffc-CSRS only in the way the data are analyzed and provides a simpler alternative. Kiefer scanning is, however, much less efficient at removing the fixed structure noise compared to the method proposed here, which only relies on a finite number of shifts to define the flat field. We will call it averaged-CSRS (a-CSRS) to differentiate it from ffc-CSRS. In the rest of this paper, we will illustrate the power of these methods on specific examples, highlighting their respective merits and problems.

EXPERIMENTAL RESULTS

Raman scattering spectra were recorded in the 90° scattering configuration, using a triple-subtractive spectrometer (T64000, Horiba Jobin-Yvon) with 1800 lines/mm gratings (blazed at ~550 nm). The solution under study (typically, a dye at micromolar concentration) was placed in a 1 cm path quartz cuvette. A $\lambda/2$ waveplate was used to adjust the polarization of the incident light to be either parallel (||) or perpendicular (⊥) to a fixed Glan-Thompson polarizer placed in collection, thereby allowing the measurement of polarized differential cross sections. A detailed schematic of the experiment is presented in the Supporting Information.

Raman Peaks in Resonance Conditions. We start with the measurement of the 595 cm^{-1} peak of Nile Blue A (NB) in water (see ref 36 for details) under resonant laser excitation at 647 nm, as illustrated in Figure 2. Although beyond the reach of most existing methods, this is a relatively "easy" case of RR scattering, since the quantum yield is ≈4% and the Raman-to-fluorescence ratio is ≈5×10^{-4}. It is nevertheless an interesting tutorial example to illustrate the method in a real application. The more challenging case of Rhodamine 6G is presented later.

For a fixed grating position, 250 spectra were acquired (in low-gain mode, to maximize the number of collected photons per spectrum without reaching saturation[36]), totalling ~10^4 counts (or equivalently 1.5×10^5 photons) at the central wavelength, for a typical total acquisition time of ~2 min. This acquisition was repeated 50 times, with cumulative shifts of 1 cm^{-1} in the grating position (a monotonous shift direction works best, minimizing spurious backlash discrepancies in wavenumbers). Figure 2a presents the 50 average spectra plotted against their respective wavenumber axes. During these experiments, it was noted that a stable laser intensity is of paramount importance if the fixed-structure noise is to be properly subtracted. For the same reason, the acquisition time was adjusted for each grating position so that the intensity of the central column of pixels was approximately constant across all spectra (the level of adjustment required depends on the slope of the fluorescence). The flat-field spectrum, characterizing the inhomogeneous response of individual CCD columns, is obtained from the averaged-along-columns spectra and provides an accurate description of the fixed-structure noise (which is clearly visible after subtraction of a polynomial fit as shown in Figure 2b). Implicit in this is the experimental fact that the fixed-structure noise of the CCD is not wavelength dependent for small shifts (~50−100 cm^{-1}) of the grating around a certain central wavelength. To ensure that this is the case, it is beneficial to bin the CCD along the spatial direction in a region contained within the entrance slit image (in usual experiments, the opposite is done, with the binning region entirely containing the slit image). This can also be checked beforehand for any given system by studying the fixed-structure

dx.doi.org/10.1021/ac301696p | Anal. Chem. 2012, 84, 7938−7945

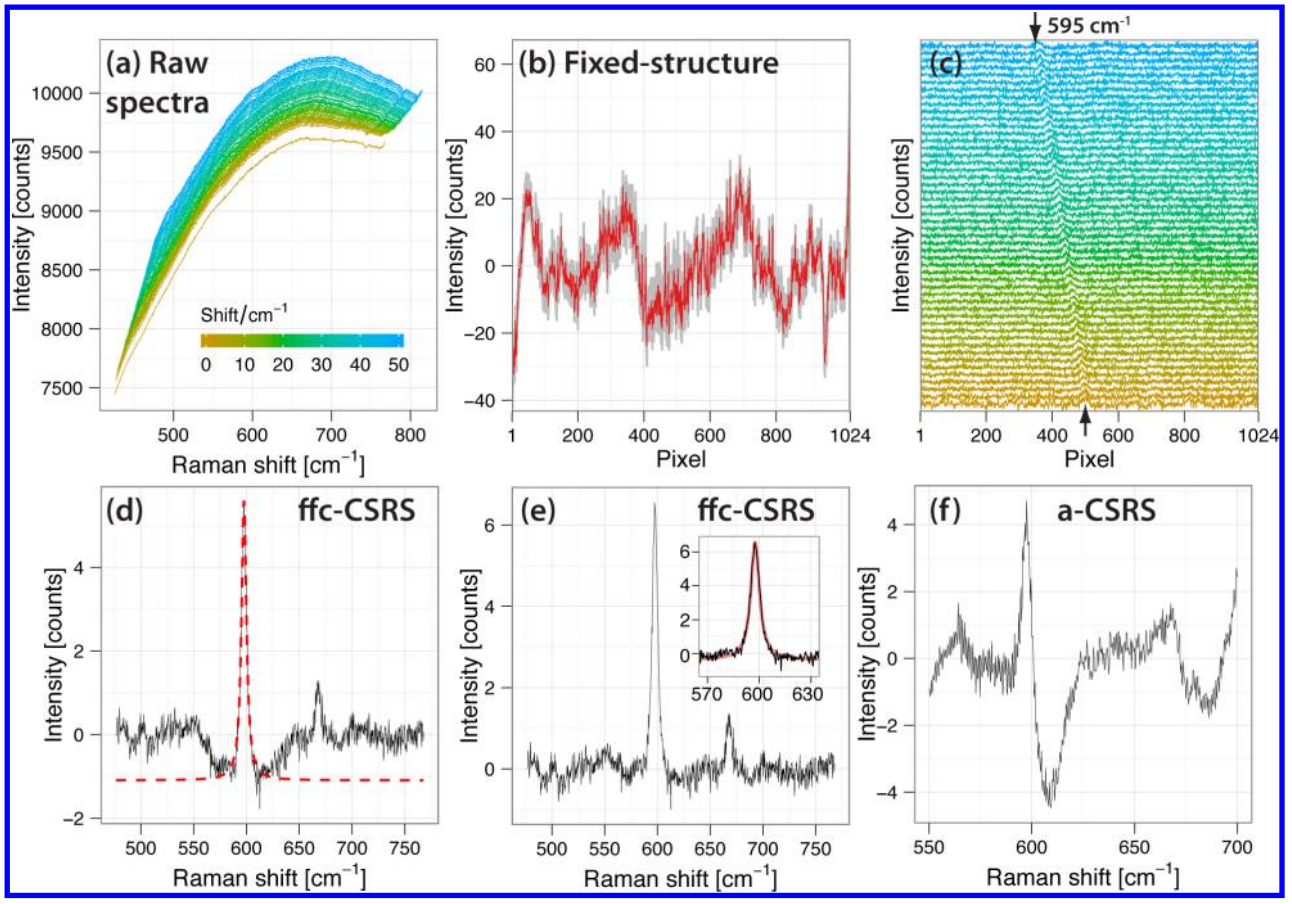

Figure 2. CSRS measurement and analysis of Nile Blue A (NB) (3 μM) in water, with parallel polarization. (a) Averages of 250 spectra obtained at 50 grating positions with 1 cm^{-1} shifts. (b) Residuals after subtraction of a fourth-order polynomial (gray lines) and for the average of all spectra against the CCD pixels used as a flat-field correction (red curve). (c) Shifted spectra after subtraction of a polynomial baseline and flat-field correction, plotted against CCD pixel columns. The shifting 595 cm^{-1} peak of NB is highlighted by the two arrows. (d) Recovered Raman spectrum after averaging of the flat-field corrected spectra. Three main peaks are visible at 500, 595, and 670 cm^{-1}; a Lorentzian fit is superimposed on the 595 cm^{-1} peak. (e) Same as in (d), with improved flat-field correction using the fitted Lorentzian as described in the Supporting Information. Inset: Lorentzian fit of the 595 cm^{-1} peak, with full width at half-maximum Γ = 6.1 cm^{-1}. (f) Direct a-CSRS average of the spectra in (a) interpolated at matching wavenumbers and background-corrected using a fourth-order polynomial.

noise at different Raman shifts.[36] A flat-field correction for each individual grating shift is then performed as described briefly earlier and in full detail in the Supporting Information. The result of this procedure is shown in Figure 2c. The 595 cm^{-1} peak of NB is now visible as a shifting feature indicated by the arrows. The average of these corrected spectra (at matching wavenumbers) is presented in Figure 2d as the fluorescence-free ffc-CSRS Raman spectrum of NB, evidencing three major peaks in the spectral window covered by the CCD and above the noise level at 500, 595, and 670 cm^{-1}, respectively.

The baseline of the spectrum is not perfectly flat, particularly in the spectral region 550−650 cm^{-1} around the most intense peak; this is because the Raman peak itself appears as a broad notch in the flat-field correction and also because of the polynomial fits carried out during the analysis. As the number of shifts increases, the importance of this predictable artifact decreases and it is often of no consequence in the final result. Nevertheless, it is possible to refine the data analysis (see Supporting Information for details) in a second iteration and avoid altogether this artifact, which can be important in detailed studies of the line shape of a peak and in the determination of its exact cross-section. The result of this refined analysis is shown in Figure 2e, clearly demonstrating the Lorentzian nature of this peak.

The ability to measure the two weak secondary peaks of NB (with Raman-to-fluorescence ratios below 10^{-4}) around the main Raman peak attests to the remarkable power of the method. Moreover, the ability to visually assess the quality of the recovered spectrum by gauging the peak intensity relative to the remaining noise level (either photon-limited or containing traces of unaccounted noise) is a substantial advantage of this technique. In comparison, fitting-based deconvolution algorithms typically used in SERDS or SSRS yield spectra devoid of noise and are more likely to have spurious spectral features which can be misinterpreted as real peaks.

Finally, it is interesting to compare these results to the more direct method of a-CSRS (inspired from Kiefer scanning), the result of which is shown in Figure 2f. The main Raman peak is again here recovered but is on top of a nontrivial background preventing any serious peak shape analysis. In addition, spurious noise in the form of high-frequency oscillations appears as a result of the extrapolation necessary to carry out the average (because spectra at different shifts have a different wavenumber scale). As a result of these effects, the two secondary Raman peaks are no longer visible. This highlights the benefit of ffc-CSRS over a-CSRS for ultrasensitive applications.

dx.doi.org/10.1021/ac301696p | *Anal. Chem.* 2012, 84, 7938−7945

It is remarkable that the method allows an accurate measurement of Raman peaks that are swamped in a fluorescence background and effectively invisible in the fixed-structure noise (which here is ~5 times larger than the primary Raman peak). We would like to re-emphasize that the measurement here is done for a single polarization (||); i.e., contrary to PD-RRS,[36] it does not involve any restriction on the polarization properties of the peak. The technique is therefore capable of retrieving precious structural and electronic information in full resonance conditions, a longstanding ambition in resonant Raman spectroscopy. We give further evidence of this in the next subsection, where measurements of complete RR spectra are presented, with lower spectral resolution.

Retrieving Complete RR Spectra. The previous example was obtained with a medium-high resolution grating (1800 lines/mm); this is important if we want to observe the true line shape of peaks and measure their widths accurately, but it is at the expense of restricting the observable window of Raman shifts on the CCD. However, measurements over a wider window where we can observe the full resonant spectrum are also possible. This latter case is important when the relative intensities of peaks are to be extracted in resonance; they contain the resonant profile of individual vibrations and, accordingly, convey precious structural information. Figure 3 shows such a measurement of NB with 568 nm laser excitation (a similar measurement at 633 nm is complicated by oxygen absorption lines as explained later) and a 600 lines/mm grating that covers the full region of fingerprint modes for this molecule. Figure 3a shows the raw (fluorescence) spectrum for this excitation wavelength, which is just above the absorption maximum of NB. This produces a situation in which the low energy side (Raman shift) of the Raman spectrum is in the tail of fluorescence while the high energy side, on the contrary, is already swamped by overwhelming fluorescence (with Raman-to-fluorescence ratios down to ~10^{-3}). A subtraction of a fourth-order polynomial, as shown in Figure 3b, already allows one to see the low frequency fingerprint mode at 595 cm^{-1}. Still, the high energy fingerprint mode at 1640 cm^{-1} is only barely visible and overwhelmed by the noise. This noise is limited by the fixed-structure noise of the CCD. Note also that the noise increases from left to right in Figure 3b, accounting for the fact that it is proportional to the intensity, i.e., the fluorescence background.

CSRS measurements were carried out with 50 shifts of 2 cm^{-1} each. A direct averaging of the shifted spectra (realigned so that their energies in Raman shifts coincide) results in the a-CSRS spectrum shown in Figure 3c. As already explained, the process of realigning the spectra and averaging discounts a substantial proportion of the fixed-structure noise, though not entirely. This allows the observation of several Raman peaks that were previously buried in the fixed-structure. Notwithstanding, we can obtain a much better result using a flat-field correction analysis (ffc-CSRS), the result of which is presented in Figure 3d. As can be appreciated, there is a superb fixed-structure noise rejection, together with a flat background that allows the observation of peaks that are a factor of ~10 smaller than the main fingerprint modes at 595 and 1640 cm^{-1}.

The ability to obtain such a detailed RR spectrum opens wide-ranging possibilities for further studies. As an example, the bare RR spectrum may be compared to the spectrum obtained in surface-enhanced Raman scattering (SERS) conditions.[40] The latter, shown in Figure 3e, was obtained for NB molecules directly adsorbed onto a metal surface (silver colloids here). Changes in relative peak intensities may be used to study adsorption effects and surface-selection rules.[41,42] The remarkable similarity between the two spectra provides a clear experimental evidence that the majority of the Raman peaks in RR conditions present the same Raman tensor symmetry,[43] which is imposed by the electronic state responsible for the RR effect.

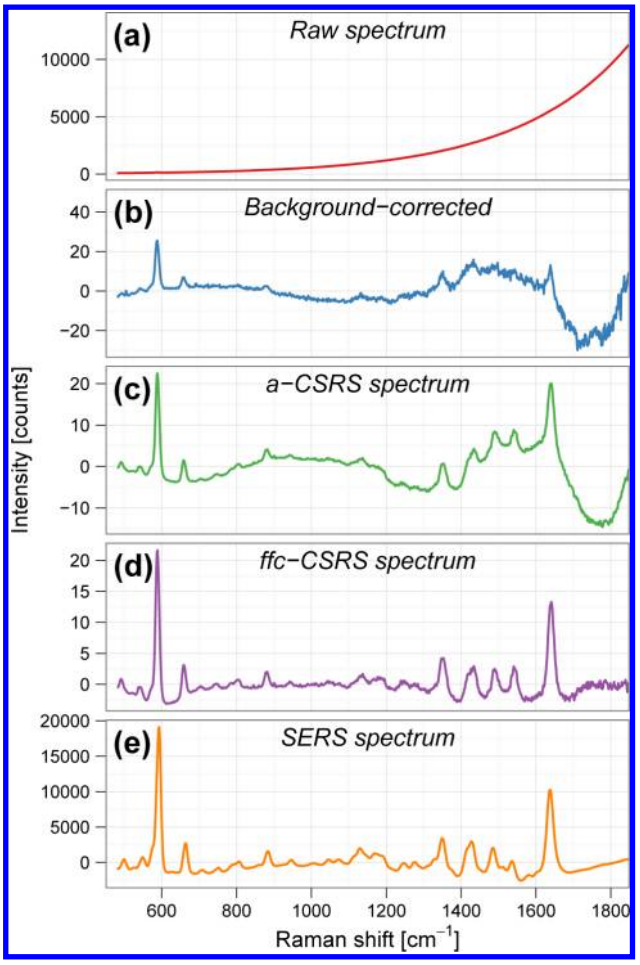

Figure 3. (a) Raw Raman + fluorescence spectrum of NB at 568 nm laser excitation and lower resolution (600 lines/mm grating). In this region, the most intense fingerprint modes of NB (595 and 1640 cm^{-1}) can still be seen (if zoomed in), but other Raman-active modes of NB are swamped in the fluorescence. (b) Subtraction of a fourth-order polynomial from the data to reveal the residual noise structure. The signal-to-noise ratio is limited by the CCD noise structure, and the weaker peaks in the region 1200−1600 cm^{-1} are not observable, regardless of the acquisition time. (c) Plain average of the shifted spectra (a-CSRS). This removes partially the fixed-structure noise and starts revealing the peaks. (d) A much better spectrum retrieval is achieved with the ffc-CSRS method introduced in this paper. Notice how the rms of the noise increases from left to right, resulting from the fact that the rms is proportional to the intensity of the background. (e) For comparison, we reproduce the SERS spectrum of NB (where the fluorescence is quenched[39]) obtained at the same laser excitation energy of 568 nm.

Resonant Depolarization Ratios. To further illustrate the potential of this technique in extremely challenging Raman-to-fluorescence intensity ratios, we present in Figure 4 the Raman spectrum of RH6G in water (with a quantum yield close to 1) at a resonant excitation wavelength of 514 nm. This is arguably

dx.doi.org/10.1021/ac301696p | Anal. Chem. 2012, 84, 7938−7945

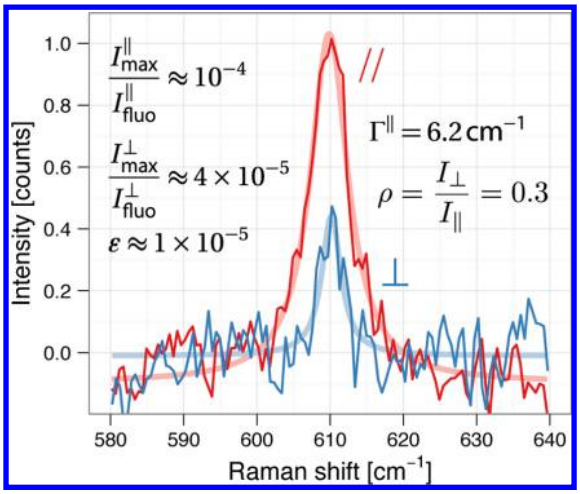

Figure 4. Fingerprint 610 cm^{-1} Raman mode of RH6G in water excited at 514 nm. Spectra are shown for both ∥ and ⊥ scattering configurations after performing the ffc-CSRS analysis based on 50 shifts of 1 cm^{-1}, each cumulating 1500 spectra. An experimental value of 0.3 results for the resonant depolarization ratio $\rho = I_{\perp}/I_{\parallel}$, in good agreement with the theoretical value expected of 1/3 at resonance for a single electronic state.[44] As far as we know, this is the first experimental determination of a depolarization ratio in full resonance for a dye with a high fluorescence quantum yield like RH6G.

one of the hardest cases in RR spectroscopy. The result of the ffc-CSRS procedure is shown for ∥ and ⊥ polarization configurations, for the region around the 610 cm^{-1} fingerprint peak of RH6G. We note that the simpler a-CSRS does not work in such a difficult case. The recently proposed technique of polarization difference[36] successfully recovered the Raman peak in this exact configuration and provided further confirmation for the estimate of the Raman cross-section (2.3 × 10^{-24} cm^2/sr). However, it should be emphasized that the polarization-difference method relies on an assumption of the depolarization ratio of the Raman mode at resonance. Herewith, such an assumption is not required, and the two independent measurements for the ∥ and ⊥ configurations can in fact be used to provide a direct measurement, and independent validation, of the depolarization ratio. The value obtained, 0.3, is in good agreement (within experimental uncertainty) with the expected theoretical value of 1/3 for a resonance with a single electronic state.[44] It also implies that the method developed here can potentially be used to measure antisymmetric components of the Raman tensor[45] in resonance conditions.

The examples presented above clearly demonstrate the power of the method for RR studies, yet RR spectroscopy is not the only situation where a small signal needs to be isolated from a much larger background. We give in the next section an additional proof of the general applicability of the method in a completely unrelated field: the study of weak absorption lines of atmospheric gases.

Short Path-Length Measurement of Weak Absorption Lines. The visible and near-IR spectrum is straggled with very weak absorption bands from gases, which are familiar to atmospheric physicists and astronomers[47] since they become important in long-path-length (∼kilometers) observations. The so-called Fraunhofer lines, seen in the emission spectrum of the sun, are one example of such bands. The relative weakness of these bands generally derives from the fact that they are electric-dipole forbidden but, for example, magnetic-dipole allowed transitions. In addition, they present complex roto-vibrational substructures in which coupling of the vibrations with the nuclear spins also needs to be considered. An example of this type of absorption is the so-called *B*-band of oxygen that occurs around 686 nm.[37] Oxygen has also another weak absorption band around ∼630 nm called "the γ-band", which is sometimes preferred for optical absorption characterization of air/mass volume in atmospheric physics experiments.[37] This is due to the fact that the γ-band has less of an overlap than the *B*-band with residual water lines. Both bands of oxygen (the *B* and γ) have been studied to a very sophisticated level of detail, and both effective Hamiltonians and appropriate phenomenological parameters for them are available in the literature to describe the spectra.[37] These bands are normally monitored by very long path length (∼20 km) ground-based instruments or by satellite observations. In our experiments, we observe the very same absorptions using an optical path of the order of ∼10 m; i.e., we compensate a much reduced optical path with a much greater sensitivity.

Figure 5 shows an example of this kind of measurement for the *B*-band of oxygen using the exact same method we have described for RR signals in the previous sections. For this particular measurement, the fluorescence of NB (in ethanol, 6 μM concentration) excited at 633 nm was used merely as a stable broadband light source (any other fluorescent source

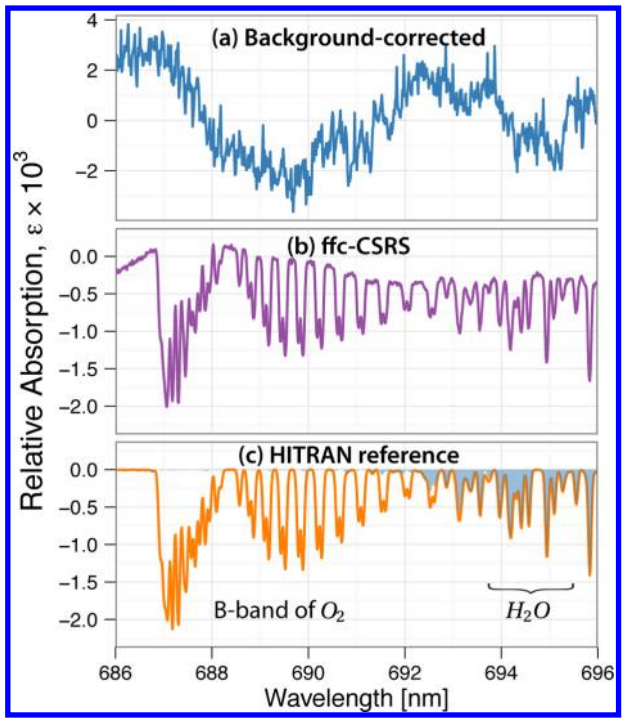

Figure 5. *B*-band of oxygen in short path-length measurements. Fluorescent light was used to monitor the weak absorption lines of atmospheric oxygen gas. (a) Residual (i.e., signal minus fourth-order polynomial fit) of the fluorescence. The signal does not reveal any spectroscopic line and is dominated by fixed-structure noise. (b) Result of the ffc-CSRS method applied with 41 shifts of 1 cm^{-1}. In (c), we show a reference spectrum calculated with the HITRAN database,[46] considering a concentration of 21% O_2 and 1.2% water (shaded blue peaks) in an atmospheric path-length of 6.5 m. Gaussian broadening (0.65 cm^{-1}) was applied to match the instrumental broadening of our spectrometer. Note the rich vibrational substructure of the *B*-band,[37] completely resolved in (b).

dx.doi.org/10.1021/ac301696p | *Anal. Chem.* 2012, 84, 7938−7945

with a smooth broad emission in the appropriate range can be used). Along the optical path, this light propagates toward and through the spectrometer, undergoing weak absorption by the environmental oxygen in the room. This absorption is usually too weak to be noticed in fluorescence spectra under normal conditions. In our T64000 Horiba Jobin-Yvon triple-subtractive spectrometer, the optical path in air for the light from the sample to the detector is ~6.5 m. For this particular measurement, we acquired 500 spectra per shift, with 41 shifts of 1 cm^{-1} each. Measurements were done in the 90°-scattering configuration in parallel polarization (as for the RR measurements).

In Figure 5a, plain averaging of the signal obtained at a single grating shift followed by background subtraction (polynomial fit) results in a spectrum dominated by the fixed-structure noise. In contrast, the ffc-CSRS spectrum (b) clearly reveals multiple absorption lines and the fine structure of the *B*-band of oxygen, as well as some water absorption lines. The remarkable details and resolution of the rotational structure of the absorption lines, down to at least 10^{-4} relative absorption, are further confirmed in Figure 5c with a reference spectrum calculated with the HITRAN database.[46] This example clearly demonstrates that the method is general and can be applied to many more areas of spectroscopy beyond resonant Raman scattering.

DISCUSSION AND CONCLUSIONS

This novel method opens up for the first time the possibility of being able to compare predictions of the many resonant and near-resonant Raman models[44,45,48] with actual experimental data that are not based on time-resolved[24] or stimulated[31] Raman spectroscopy. In particular, several aspects of the data in this method, like the resolution with which Raman peak widths and lineshapes can be measured, are unrivalled by time-resolved techniques. There is in principle no limit to how low the rejection level can be pushed by accumulating more spectra, even though smaller and subtler forms of noise might take over at some point and limit again the photon statistics. We estimate that the maximum achievable rejection of the method, as it stands in our proof-of-principle implementation, is of the order of ~10^{-5} and could potentially reach ~10^{-6} with further refinements.

The ffc-CSRS method presented here together with the polarization difference technique, introduced in ref 36, complement each other in many circumstances for ultrasensitive Raman spectroscopy in the presence of strong fluorescent backgrounds. In particular, we observed that RR measurements in the red part of the visible spectrum can be affected by the weak absorption lines of O_2 evidenced earlier. ffc-CSRS spectra then present a superposition of these lines with the real RR spectrum, which may complicate the analysis. In contrast, PD-RRS is not affected by these lines (they cancel out in the difference spectrum) and may therefore be preferred. Alternatively, one could perform the ffc-CSRS experiments under a nitrogen atmosphere, which although less practical, is not impossible. In the absence of absorption lines, ffc-CSRS will be generally preferable, with marginally higher sensitivity; it also allows independent confirmations of the depolarization ratio which may contain information of the resonance condition[44,45,48] and/or on the presence of antisymmetric components of the Raman tensor.[45]

We close this discussion with a practical note on the applicability of ffc-CSRS in more conventional single-stage spectrometers, relying on notch filters for the rejection of stray laser light rather than a triple-subtractive spectrometer as used in our previous experiments. As detailed in the Supporting Information, simple precautions are required to circumvent the limitations of standard notch filters, which introduce wavelength-dependent oscillations if no special care is taken. With this caveat in mind, we found the method applicable in both types of spectrometers. The proposed method has a wide range of applicability and does not rely on a difference of polarization properties between the signal of interest and the background. It provides a general method to detect very small signals on a large background, which can be ~10^3–10^5 times larger than the signal itself. The case of resonant Raman scattering of dyes with moderate or high fluorescence quantum yield provides a textbook example, traditionally deemed to be extremely difficult or impossible with conventional spectrometers. The method presented in this paper, possibly complemented by the one introduced in ref 36, shows that this is not the case, and resonant Raman spectra, peak lineshapes, and cross sections are indeed obtainable if the right experimental procedures are employed to recover the photon-noise limited signal beyond fixed-structure noise.

Overall, we feel we have presented enough proof to debunk once and for all the myth that Raman spectroscopy in full resonance is beyond the realms of conventional Raman systems.[14] We believe this method will have wide-ranging applications, not only for RR spectroscopy but also in other spectroscopic areas where tiny peaks need to be measured on top of large backgrounds. Possible extensions of the method to the processing of 2D CCD images (to recover spatial features below the fixed-structure noise of the camera) are also envisioned.

ASSOCIATED CONTENT

Supporting Information

Detailed description of the flat-field correction technique, illustration of the major sources of noise in CCD-based measurements, and schematic of the experimental setup with further discussion of single-stage spectrometers. This material is available free of charge via the Internet at http://pubs.acs.org/.

AUTHOR INFORMATION

Corresponding Author

*E-mail: eric.leru@vuw.ac.nz (E.C.L.R.); pablo.etchegoin@vuw.ac.nz (P.G.E.).

Notes

The authors declare no competing financial interest.

ACKNOWLEDGMENTS

E.C.L.R. is indebted to the Royal Society of New Zealand (RSNZ) for support through a Marsden Grant and Rutherford Discovery Fellowship. P.G.E. acknowledges support from a Marsden Grant of the RSNZ. B.A. thanks S.A. Meyer for his help with the SERS measurement.

REFERENCES

(1) Mosier-Boss, P. A.; Lieberman, S. H.; Newbery, R. *Appl. Spectrosc.* **1995**, *49*, 630–638.

(2) da Silva Martins, M. A.; Ribeiro, D. G.; dos Santos, E. A. P.; Martin, A. A. A.; Fontes, A.; da Silva Martinho, H. *Biomed. Opt. Express* **2010**, *1*, 617–626.

(3) Bell, S. E. J.; Bourguignon, E. S. O.; Dennis, A. C.; Fields, J. A.; McGarvey, J. J.; Seddon, K. R. *Anal. Chem.* **2000**, *72*, 234–239.

(4) Rosi, F.; Paolantoni, M.; Clementi, C.; Doherty, B.; Miliani, C.; Brunetti, B.; Sgamellotti, A. *J. Raman Spectrosc.* **2010**, *41*, 452−458.
(5) Bell, S.; Bourguignon, E.; O'Grady, A.; Villaumie, J.; Dennis, A. *Spectrosc. Eur.* **2002**, *14*, 17−20.
(6) Bell, S.; Bourguignon, E.; Dennis, A. *Analyst* **1998**, *123*, 1729−1734.
(7) Li, Q.; Wang, K. R.; Wang, S. X. A New Approach for Fluorescence Subtraction in Raman Spectroscopy. In *CLEO:2011-Laser Applications to Photonic Applications*; OSA Technical Digest (CD), Optical Society of America, 2011
(8) Zhang, D.; Ben-Amotz, D. *Appl. Spectrosc.* **2000**, *54*, 1379−1383.
(9) Raffaëlly, L.; Champagnon, B. *J. Raman Spectrosc.* **2007**, *38*, 1242−1245.
(10) Hasegawa, T.; Nishijo, J.; Umemura, J. *Chem. Phys. Lett.* **2000**, *317*, 642−646.
(11) Zhang, Z.-M.; Chen, S.; Liang, Y.-Z.; Liu, Z.-X.; Zhang, Q.-M.; Ding, L.-X.; Ye, F.; Zhou, H. *J. Raman Spectrosc.* **2010**, *41*, 659−669.
(12) Lieber, C.; Mahadevan-Jansen, A. *Appl. Spectrosc.* **2003**, *57*, 1363−1367.
(13) Osticioli, I.; Zoppi, A.; Casteilucci, E. *J. Raman Spectrosc.* **2006**, *37*, 974−980.
(14) Myers Kelley, A. *J. Phys. Chem. A* **2008**, *112*, 11975−11991.
(15) Matousek, P.; Towrie, M.; Parker, A. *Appl. Spectrosc.* **2005**, *59*, 848−851.
(16) Friedman, J. M.; Hochstrasser, R. M. *Chem. Phys. Lett.* **1975**, *33*, 225−227.
(17) Maiwald, M.; Erbert, G.; Klehr, A.; Kronfeldt, H.-D.; Schmidt, H.; Sumpf, B.; Tränkle, G. *Appl. Phys. B: Lasers Opt.* **2006**, *85*, 509−512.
(18) Osticioli, I.; Zoppi, A.; Castellucci, E. *Appl. Spectrosc.* **2007**, *61*, 839−844.
(19) Zhao, J.; Carrabba, M.; Allen, F. *Appl. Spectrosc.* **2002**, *56*, 834−845.
(20) Oshima, Y.; Komachi, Y.; Furihata, C.; Tashiro, H.; Sato, H. *Appl. Spectrosc.* **2006**, *60*, 964−970.
(21) Kamogawa, K.; Fujii, T.; Kitagawa, T. *Appl. Spectrosc.* **1988**, *42*, 248−254.
(22) Demas, J. *Anal. Chem.* **1985**, *57*, 538−545.
(23) O'Grady, A.; Dennis, A.; Denvir, D.; McGarvey, J.; Bell, S. *Anal. Chem.* **2001**, *73*, 2058−2065.
(24) Efremov, E.; Buijs, J.; Gooijer, C.; Ariese, F. *Appl. Spectrosc.* **2007**, *61*, 571−578.
(25) Efremov, E.; Ariese, F.; Gooijer, C. *Anal. Chim. Acta* **2008**, *606*, 119−134.
(26) Long, D. A. *The Raman effect, a unified treatment of the theory of Raman scattering by molecules*; John Wiley & Sons Ltd.: Chichester, 2002.
(27) Arguello, C. A.; Mendes, G. F.; Leite, R. C. C. *Appl. Opt.* **1974**, *13*, 1731−1732.
(28) Angel, S. M.; DeArmond, M. K.; Hanck, K. W.; Wertz, D. W. *Anal. Chem.* **1984**, *56*, 3000−3001.
(29) McCreery, R. L. *Raman Spectroscopy for Chemical Analysis*; John Wiley & Sons, Inc.: New York, 2005.
(30) Shim, S.; Stuart, C. M.; Mathies, R. A. *ChemPhysChem* **2008**, *9*, 697−699.
(31) Kukura, P.; McCamant, D. W.; Mathies, R. A. *J. Phys. Chem. A* **2004**, *108*, 5921−5925.
(32) Lee, S.-Y.; Zhang, D.; McCamant, D. W.; Kukura, P.; Mathies, R. A. *J. Chem. Phys.* **2004**, *121*, 3632−3642.
(33) Kukura, P.; Yoon, S.; Mathies, R. A. *Anal. Chem.* **2006**, *78*, 5952−5959.
(34) McCamant, D. W.; Kukura, P.; Mathies, R. A. *Appl. Spectrosc.* **2003**, *57*, 1317−1323.
(35) McCain, S.; Willett, R.; Brady, D. *Opt. Express* **2008**, *16*, 10975−10991.
(36) Le Ru, E. C.; Schroeter, L.; Etchegoin, P. G. *Anal. Chem.* **2012**, *84*, 5074−5079.
(37) Gordon, I. E.; Rothman, L. S.; Toon, G. C. *J. Quant. Spectrosc. Radiat. Transfer* **2011**, *112*, 2310−2322.
(38) Deckert, V.; Kiefer, W. *Appl. Spectrosc.* **1992**, *46*, 322−328.
(39) Meyer, S. A.; Le Ru, E. C.; Etchegoin, P. G. *J. Phys. Chem. A* **2010**, *114*, 5515−5519.
(40) Le Ru, E. C.; Etchegoin, P. G. *Principles of Surface Enhanced Raman Spectroscopy and Related Plasmonic Effects*; Elsevier: Amsterdam, 2009.
(41) Le Ru, E. C.; Meyer, M.; Blackie, E.; Etchegoin, P. G. *J. Raman Spectrosc.* **2008**, *39*, 1127−1134.
(42) Le Ru, E. C.; Meyer, S. A.; Artur, C.; Etchegoin, P. G.; Grand, J.; Lang, P.; Maurel, F. *Chem. Commun.* **2011**, *47*, 3903−3905.
(43) Buchanan, S.; Le Ru, E. C.; Etchegoin, P. G. *Phys. Chem. Chem. Phys.* **2009**, *11*, 7406.
(44) Nafie, L. A. *Chem. Phys.* **1996**, *205*, 309−322.
(45) Nestor, J.; Spiro, T. G. *J. Raman Spectrosc.* **1973**, *1*, 539−550.
(46) Rothman, L.; et al. *J. Quant. Spectrosc. Radiat. Transfer* **2009**, *110*, 533−572.
(47) Cooper, P.; Johnson, R.; Quickenden, T. *Planet. Space Sci.* **2003**, *51*, 183−192.
(48) Stock, G.; Domcke, W. *J. Phys.: Condens. Matter* **1990**, *93*, 5496−5509.

Supplementary Information for: "Tiny Peaks vs Mega Backgrounds: a General Spectroscopic Method with Applications in Resonant Raman Scattering and Atmospheric Absorptions"

Baptiste Auguié,[1] Antoine Reigue,[1,2] Eric C. Le Ru,[1] and Pablo G. Etchegoin[1]

[1] *The MacDiarmid Institute for Advanced Materials and Nanotechnology School of Chemical and Physical Sciences Victoria University of Wellington PO Box 600, Wellington, 6140, New Zealand.*

[2] *ICFP, Département de Physique de l'ENS, 24 rue Lhomond, 75005 Paris, France*

I. SOURCES OF NOISE AFFECTING CCD ACQUISITIONS

CCD acquisitions of weak optical signals are generally affected by a number of noise contributions[1,2], which can limit the ultimate level of detection. The simulated data presented in Fig. 1 illustrate the problem faced in resonant Raman scattering experiments, where a strong luminescent background yields considerable shot-noise, as well as a fixed-pattern noise structure across the CCD array resulting from the inhomogeneous response of individual pixels. The purpose of this work is to present a flat-field correction scheme that removes the fixed-structure noise contribution, regaining photon-limited statistics where long averaging times can be used to arbitrarily increase the signal-to-noise ratio.

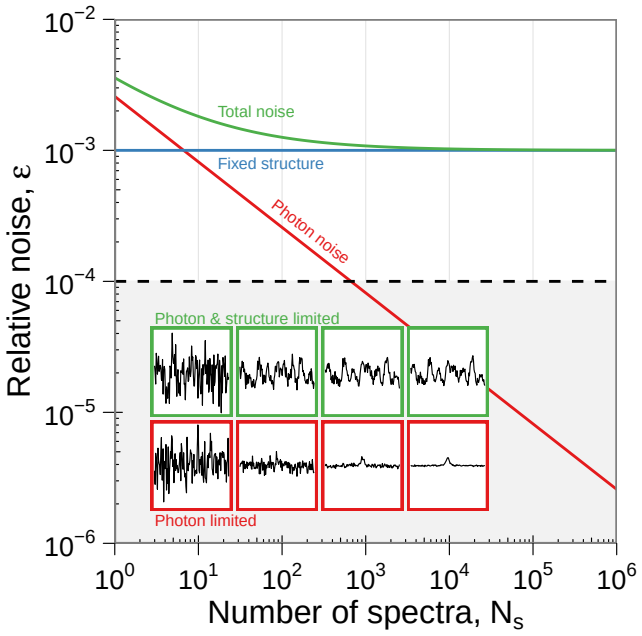

FIG. 1: Theoretical contributions to the relative rms noise ϵ affecting CCD measurements of RR spectra. The main plot presents in log-log coordinates the contributions of photon-noise (red line) and fixed structure noise (blue horizontal line), as well as their sum (green curve)[1]. In comparison, the horizontal dashed line indicates the minimum noise level limit that should be reached to resolve Raman peaks of high quantum yield dyes at resonance. Insets present simulated spectra with typical experimental parameters ($\epsilon = 10^{-3}$ for fixed-structure noise, 10^4 counts/spectra or equivalently 1.5×10^5 photons, with a typical CCD gain of 15 photons/count/pixel, Raman peak of amplitude 5 counts, plus random Gaussian noise), with a common scale, for an increasing number of averaging counts (10^1, 10^2, 10^3, and 10^4 spectra respectively). The top row contains contributions from both the fixed structure and photon noise, while the bottom row has no contribution from the fixed structure and reveals the Raman peak for $N_s \geq 10^3$.

II. FLAT-FIELD CORRECTION: METHODOLOGY

We illustrate the principles of the technique proposed in the main paper on a simulated dataset, as shown in Fig. 2. This allows us to compare the shape and intensity of a recovered Raman peak with the original data used in the simulation, thus quantifying the degree of distortion introduced by the data processing in an ideal case. We will denote by I_n the average spectrum obtained for a given shift, indexed by $n = 1 \ldots N$, where N is the number of shifts. These spectra can be viewed either as a function of CCD pixel, i.e. $I_n(p)$ with $p = 1 \ldots 1024$ in our CCD; or as a function of wavelength, i.e. $I_n(\lambda)$, where λ is implicitly a function of p at a given grating shift, i.e. $\lambda \equiv \lambda_n(p)$. In our experiments, we may write (ignoring photon-noise):

$$I_n(p) = \left[F\left(\lambda_n(p)\right) + R\left(\lambda_n(p)\right)\right] \cdot \left(1 + S_n(p)\right), \qquad (1)$$

where $F + R$ represents the signal (Fluorescence background + Raman) and the factor $1 + S$ (with $S \ll 1$) accounts for the fixed-structure noise of the CCD. F and R are independent of grating shift when expressed as a function of λ, while S is independent of grating shift when expressed as a function of CCD pixel.

The data presented in Fig. 2a were simulated to closely resemble the experimental conditions:

- $F(\lambda)$ is taken as a fourth-order polynomial in wavenumbers (with mean value around $\sim 10^4$ counts);
- $R(\lambda)$ is a Lorentzian function representing a Raman peak of magnitude 5 counts and full-width at half

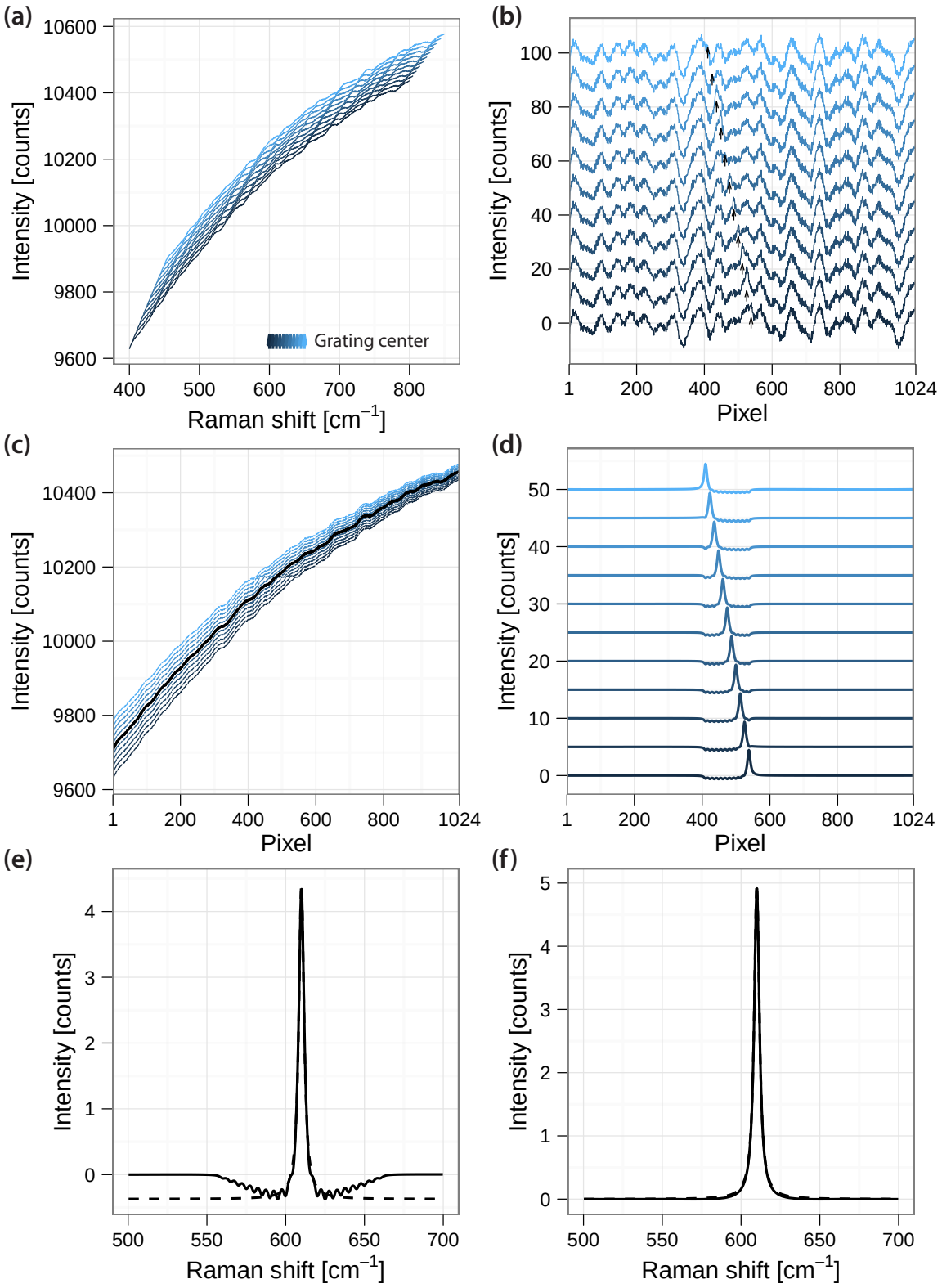

FIG. 2: Peak-retrieval methodology on simulated data. (*a*) Simulated spectra according to Eq. 1, with 11 shifts of 5 cm^{-1} each (vertically offset for clarity). (*b*) Spectra after removal of a 4th-order polynomial; offset for clarity. A black arrow indicates the position of the Raman peak, invisible in the constant fixed-structure noise. (*c*) Same as in (*a*), plotted against CCD pixels. The black curve is the average of all spectra, defined in the text as the flat-field correction. Spectra are not artificially offset here, it is the shift of the fluorescence that produces the regular offset. (*d*) Recovered spectra after flat-field correction. (*e*) Average spectrum from (*d*), plotted against wavenumbers. The dashed line is a Lorentzian fit to the peak in the region 590 cm^{-1}–630 cm^{-1} (parameters: peak position 610 cm^{-1}, width 3.91 cm^{-1}, intensity 4.81 counts). (*f*) Recovered peak after a second-step background subtraction, as described in the text. The dashed line is the original Lorentzian used in the simulation.

maximum (FWHM) $4\,\mathrm{cm}^{-1}$, centred at $610\,\mathrm{cm}^{-1}$;

- $S(p)$ is a fixed-structure noise component (with respect to the pixels) of maximum amplitude 10^{-3}, created by 10 Fourier components of randomly selected amplitudes and frequencies.

In Fig. 2, $N = 11$ spectra are presented with shifted central position and offset for clarity. The weak Raman peak is completely buried in the fixed-structure noise, as can be appreciated from the ratio of magnitudes of R/S. In Fig. 2b the same spectra are presented after simple background correction, i.e. removal of a smooth fourth-order polynomial to subtract the fluorescence background. The pixel position of the Raman peak is indicated by small arrows for each of the offset spectra, but is essentially invisible because of the fixed-structure noise.

Our peak-retrieval procedure is constructed from a flat-field reference spectrum, which contains the pixel-dependent fixed-structure noise that masks the Raman peak. This flat-field, shown in Fig. 2c (black curve), is obtained from the averaged-along-pixel intensity of all spectra:

$$I_{\mathrm{FF}}(p) = \frac{1}{N}\sum_{n=1}^{N} I_n(p). \tag{2}$$

The following step consists in subtracting this flat-field correction to each of the 11 individual spectra. A direct subtraction is not optimal, it would not suppress efficiently the fixed-structure noise because it is proportional to the fluorescence background level, which varies in intensity across the CCD pixels for different positions of the grating (note the vertical separation between spectra in Fig. 2c). Instead, a weighted difference is applied, minimising the residual (difference) $D_n(p)$ between an individual spectrum and the flat-field:

$$D_n(p) = I_n(p) - \left(\sum_{j=0}^{d} a_j p^j\right) \cdot I_{\mathrm{FF}}(p), \tag{3}$$

where a_j are polynomial coefficients. We found that a 4th-order polynomial ($d = 4$) produces a satisfactory fit between the intensity levels of the two spectra in all our experiments, with only minute residual oscillations. The results of this polynomial-weighted subtraction are displayed in Fig. 2d for each of the N individual spectra (offset vertically for clarity). Very prominently, the feature of the Raman peak stands out (at different pixel positions), and the fixed-structure noise has been totally eliminated.

The last step of this analysis consists of combining the N individual corrected spectra (D_n) of Fig. 2d. This process requires interpolation of the spectra at matching wavenumbers, and averaging their intensity in the spectral region where they all overlap,

$$D(\lambda) = \frac{1}{N}\sum_{n=1}^{N} D_n(\lambda). \tag{4}$$

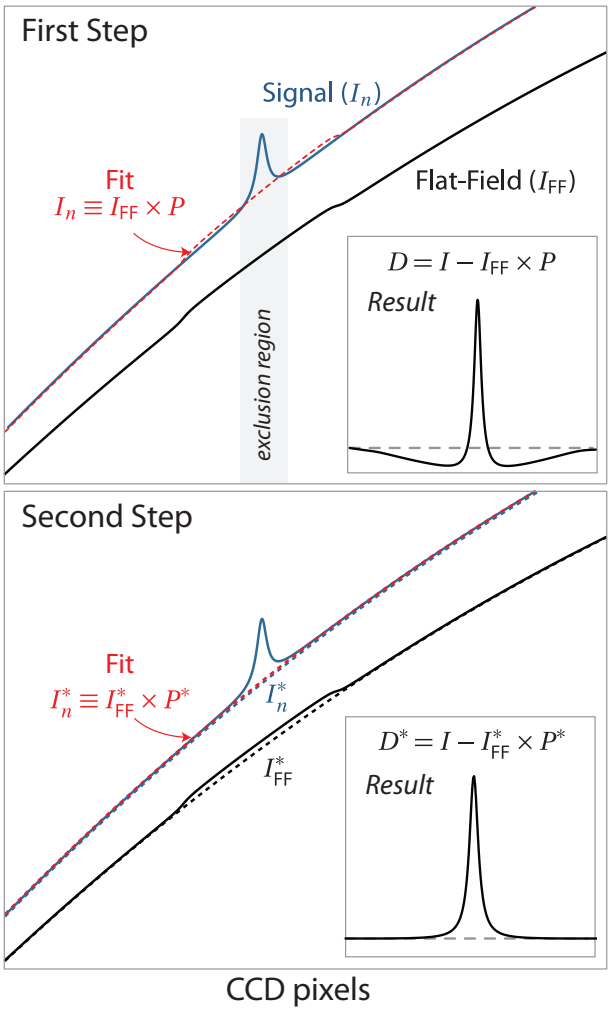

FIG. 3: Schematic illustration of the weighted subtraction performed as flat-field correction. (Top) A spectrum (I_n) containing a slowly-varying fluorescence background and a Raman peak (exaggerated for clarity) is represented by the blue curve. The flat-field (I_{FF}), obtained from the average of 50 such spectra at shifted grating positions is shown as a black curve. Note that the fluorescence background is not identical in both curves, due to the spectral variation of the fluorescence intensity. In order to match the intensities of I_n and I_{FF} across the CCD, and therefore the fixed-structure noise, the subtraction of the flat-field is weighted by a low-order polynomial P according to Eq. 3. The presence of a strong Raman peak can distort the fit (red dashed curve); when applicable it is often preferable to exclude a spectral region around isolated Raman peaks (grey shaded area). Inset: result of averaging the difference spectra in the overlapping spectral region. Note the negative baseline around the peak. (Bottom) Improved analysis from the initial result. A new series of spectra, such as I^*_n (dashed blue curve), is obtained by subtracting the result of the first analysis (either a Lorentzian fit of the Raman peak, or the actual spectrum itself). From these data, a flat-field I^*_{FF} is derived (dashed black curve), that does not have the artefact of the multiply-shifted Raman signals. The fit required to match the intensities of signal and flat-field is performed between the peak-removed signal I^*_n and flat-field I^*_{FF}; the coefficients of the polynomial P^* are used to perform the weighted difference. Inset: corrected result with flat baseline.

The resulting spectrum $D(\lambda)$ is shown in Fig. 2e, together with a best-fit Lorentzian of the Raman peak. The fit parameters (peak position $610\,\mathrm{cm}^{-1}$, width $3.91\,\mathrm{cm}^{-1}$, intensity 4.81 counts), limited to the region $590\,\mathrm{cm}^{-1}$–$630\,\mathrm{cm}^{-1}$, are in good agreement with the original function used in the simulated data. However, due to the finite number of shifts, the flat-field correction not only contains the fixed-structure noise, but also a periodically repeated trace of the Raman peak, evidenced as a small negative dip around the peak in the spectra of Fig. 2e. In addition, the polynomial fit in Eq. 3 also attempts to partially fit the Raman peak, which further amplifies this negative dip. These effects, artificially amplified for the sake of illustration in Fig. 3, are almost negligible when the range of grating shifts is sufficient and when studying full Raman spectra containing several Raman peaks.

For accurate determination of line-shape, line-width, and cross-section of a single Raman peak, it is however desirable to remove this artefact. To do so, a simple procedure can be applied to recover a flat baseline and the true lineshape of the peak. To this end, the fitted Lorentzian of Fig. 2e (or alternatively the spectrum of Fig. 2e itself) is subtracted to the original N spectra and we reiterate all the same steps with this new flat-field, I^*_{FF} (that ideally does not contain the spurious pattern due to the shift-repeated Raman peak)[3]. As a result, we obtain the final spectrum shown in Fig. 2f, together with the ideal solution. The new fitted parameters (peak position $610\,\mathrm{cm}^{-1}$, width $3.99\,\mathrm{cm}^{-1}$, intensity 4.97 counts) confirm this excellent agreement. The same procedure could be applied to multiple peaks simultaneously, as in the case of Nile Blue (NB) in the main paper, and could also be reiterated for improved accuracy (each step yielding a more accurate fit result, that can be repeatedly subtracted from the original flat-field). The implementation of such corrections is further illustrated in Fig 3.

III. SCHEMATIC OF THE EXPERIMENT AND PRACTICAL CONSIDERATIONS FOR SINGLE-STAGE SPECTROMETERS

A very schematic representation of the triple subtractive Raman spectrometer used in this experiments (T64000, Horiba Jobin-Yvon) is shown in Fig. 4. The layout is schematic because the real spectrometer involves two stages of mirrors at different heights, and the gratings work with dispersion in the vertical (rather than horizontal) direction. Nevertheless, the layout in Fig. 4 conveys the basics: a double subtractive spectrometer that acts as a "tuneable notch-filter" followed by a triple dispersive stage. The double and triple stages must work in synchronisation during wavelength scans, for we found that if they are decoupled it results in an unsatisfactory cancellation of fixed-structure noise for our purposes.

A thick Glan-Thompson polariser is used at the entrance of the spectrometer, to avoid Fabry-Perot oscillations in the detected signal[1]. The scattering configuration is at 90° and the incident linear polarisation can be selected by a $\lambda/2$-waveplate in the incoming beam. The Glan-Thompson polariser is fixed in the vertical direction, which corresponds to the maximum efficiency of the gratings. The image of the laser crossing the cuvette (where the dye is) fills the entrance slit of the spectrometer along the direction of the slit (horizontal).

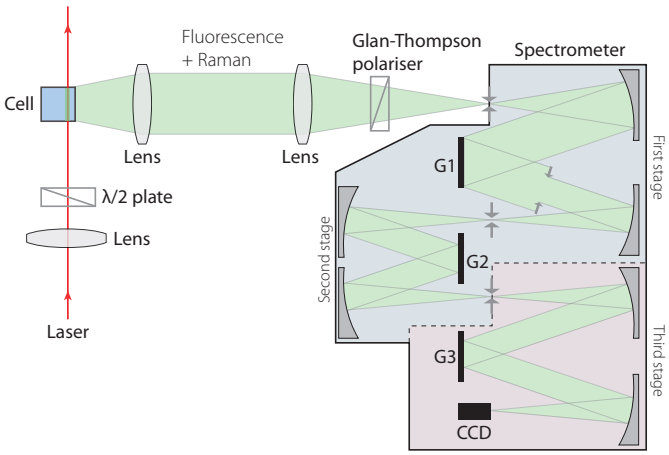

FIG. 4: Schematic representation of the triple subtractive spectrometer, and the 90° scattering configuration used in our experiments. See the text for further details.

The biggest advantage of a triple subtractive spectrometer for RR spectroscopy is the fact that it avoids the use of notch filters[2]. The implementation in single-stage, notch-filter based spectrometers requires a few additional considerations. This is because in addition to the fixed-structure noise of the CCD, the transfer functions of notch filters are in general not spectrally flat – they typically display oscillations as side-bands of the rejection window. Contrary to the fixed-structure noise, these oscillations are wavelength-dependent, like the Raman signals, and therefore do not cancel out in ffc-CSRS, as shown in Fig. 5a. There are two options to remedy this problem. The first one is to use background-removal procedures (as shown in the inset of Fig. 5a) to remove these oscillations from the CSRGS spectrum (since they are smooth and devoid of fixed-structure noise). The second option would be to use a specially-designed notch filter with no oscillations. Conveniently, we found a much simpler alternative, which consists in replacing the notch filter with a mere beam-splitter. For measurement in solutions with an immersion objective, we found that this non-standard approach did not result in substantial stray light problems – the amount of back-scattered stray light is minimal – allowing for the recovery of the ffc-CSRS spectrum of NB in water devoid of notch oscillations, shown in Fig. 5 (inset). This demonstrates the applicability of the method in the majority of existing Raman spectrometers.

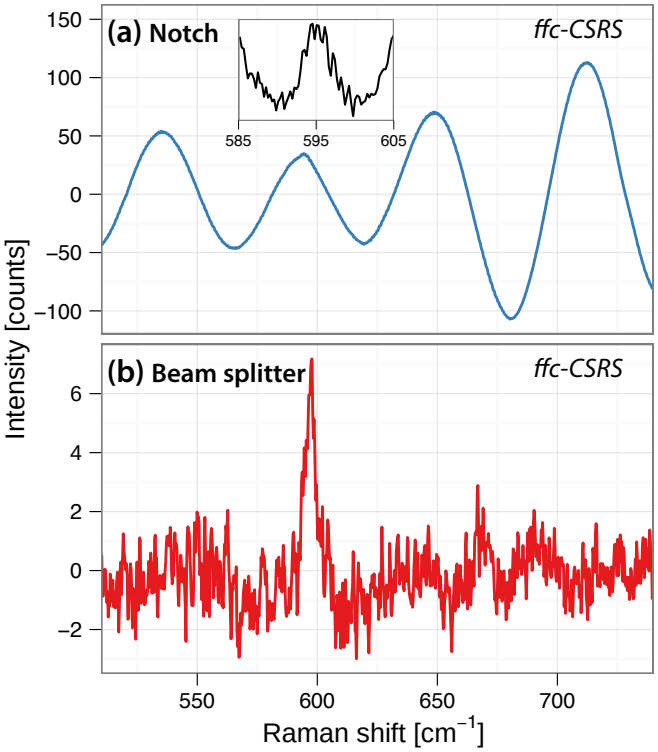

FIG. 5: ffc-CSRS method with a single-stage Raman spectrometer (LabRam, Horiba Jobin-Yvon). A 5 µM solution of NB in water was probed using a ×20 immersion objective, at a wavelength of 633 nm (HeNe). (a) Result of the analysis after 50 shifts of 2 cm^{-1}. Strong oscillations are attributed to the transfer function of the notch filter. The inset reveals the 595 cm^{-1} peak of NB, after subtraction of a fourth-order polynomial around the peak. (b) Result of the ffc-CSRS analysis of 50 shifts of 2 cm^{-1} acquired with a beamsplitter replacing the normal notch filter.

[1] Le Ru, E. C., Schroeter, L. & Etchegoin, P. G. Direct measurement of resonance Raman spectra and cross-sections by a polarization difference technique. *Anal. Chem.* **84**, 5074–5079 (2012).

[2] McCreery, R. L. *Raman Spectroscopy for Chemical Analysis* (John Wiley & Sons, Inc., 2005).

[3] Zhao, J., Lui, H., McLean, D. I. & Zeng, H. Automated autofluorescence background subtraction algorithm for biomedical Raman spectroscopy. *Appl. Spectrosc.* **61**, 1225–1232 (2007).